IEEE Access
Multidisciplinary | Rapid Review | Open Access Journal

Received 24 March 2024, accepted 9 April 2024, date of publication 12 April 2024, date of current version 19 April 2024.

Digital Object Identifier 10.1109/ACCESS.2024.3387909

RESEARCH ARTICLE

Modeling and Stability Analysis of an Active Islanding Detection Method in DC Microgrids Using Real-Time Wavelet Analysis

ELMIRA KAZEMINIA, (Student Member, IEEE), SAJJAD GOUDARZITAEMEH, (Graduate Student Member, IEEE), SUZAN EREN, (Senior Member, IEEE), AND ALIREZA BAKHSHAI, (Fellow, IEEE)
Department of Electrical and Computer Engineering, Queen's University, Kingston, ON K7L 3N6, Canada
Corresponding author: Elmira Kazeminia (16ek6@queensu.ca)

ABSTRACT This paper presents a new real-time method for fast and reliable detection of islanding events in DC microgrids (MGs). The method involves injecting a distinct periodic perturbation signal from the controller of the main bidirectional dual active bridge (DAB) DC-DC converter at predetermined intervals. This discrete signal significantly reduces its impact on power quality. Intentionally injecting a narrow-band perturbation signal enhances the method's ability to differentiate islanding events from random fluctuations and disturbances, demonstrating its robustness. Decentralized detectors at each MG sub-DC link monitor system parameters. Real-time wavelet analysis concurrently decides to disconnect the main DC grid and common DC bus during islanding events, eliminating the need for complex DC circuit breakers (CBs). The proposed method is easily implementable without requiring a separate communication infrastructure and is applicable in scenarios with or without power exchange between the main DC grid and MGs. Detailed mathematical stability analysis confirms the method's stability, aligning with the IEEE 1547 Standard, and is supported by extensive simulation results.

INDEX TERMS Active islanding detection method, DC microgrid, bidirectional DC-DC converter, high-frequency injection, islanding condition, real-time wavelet analysis, dual active bridge (DAB) converter.

I. INTRODUCTION

Recently, DC MGs have attracted attention for their greater reliability and efficiency compared to traditional AC MGs [1]. They are also noted for being more economical, providing better control and flexibility, and improving power quality [2]. While DC MGs offer numerous benefits, the challenge of detecting islanding conditions remains complex. In DC MGs, unlike AC power systems, there are no parameters like frequency or reactive power, which are commonly used in IDMs for AC MGs. This lack of reactive power, while beneficial in some ways, means traditional IDMs utilized in AC power systems cannot be applied to DC MGs. Moreover, DC MGs cannot employ different frequency-based detection techniques such as rate of change of frequency (ROCOF), active frequency drift (AFD), and slip mode frequency shift (SMS), limiting detection strategies to voltage and current monitoring [3], [4], [5], [6]. This limitation poses challenges in accurately identifying islanding events, especially when power generation closely matches consumption. Additionally, the complexity of protection systems in DC MGs, due to the lack of zero-crossing current, necessitates the development of fast and reliable detection methods, highlighting the need for innovative approaches in DC MGs.

Generally, IDMs are categorized into local and remote approaches. Local IDMs monitor system parameters at the point of common coupling (PCC) to detect islanding

The associate editor coordinating the review of this manuscript and approving it for publication was Santu Giri.

© 2024 The Authors. This work is licensed under a Creative Commons Attribution-NonCommercial-NoDerivatives 4.0 License.
For more information, see https://creativecommons.org/licenses/by-nc-nd/4.0/

TABLE 1. Comparison of traditional islanding detection methods in AC/Hybrid power systems.

Categories	Ref.	IDM	DT	Power Quality	Error Detection Rate	NDZ
Local Conventional Passive IDM	[10]	Under/Over Voltage Protection	4 ms - 2 s	No Impact	High	Large
	[10]	Under/Over Frequency Protection	4 ms - 2 s	No Impact	High	Large
	[11]	Rate of Change of Frequency	24 ms	No Impact	High	Large
	[12]	Rate of Change of Frequency Over Power	100 ms	No Impact	Low	Smaller than ROCOF
	[13]	Rate of Change of Power	24-26 ms	No Impact	Low	Smaller than OUV/OUF
	[14]	Voltage Unbalance	0.053 s	No Impact	Low	Large
	[15]	Phase Jump Detection	10-20 ms	No Impact	High	Large
	[14]	Total Harmonic Distortion	45 ms	No Impact	High	Large
Local Conventional Active IDM	[4], [5]	Active Frequency Drift	2 s	Degrade	Low	NDZ increases with increasing of Q
	[16]	Active Frequency Drift with Positive Feedback	2 s	Degrade	Low	Smaller than AFD
	[17]	Sandia Frequency Shift	0.5 s	Slightly degrade	Low	Smallest
	[17]	Sandia Voltage Shift	0.5 s	Slightly degrade	Low	Smallest
	[18]	Slip Mode Frequency Shift	0.4 s	Have an impact on system transient Stability	Low	Smaller than AFD
	[19]	Impedance Measurement	0.77 s – 0.95 s	Produce harmonics	Low	Small NDZ for single System
Hybrid IDMs	[20]	Voltage Unbalance, Sandia Frequency Shift, and Sandia Voltage Shift	-	Reduce negative impact	None	Very small
	[21]	Rate of Change of Frequency and Impedance Measurement	0.216 s	-	Low	Small
Local Modern Passive IDMs	[22]	Fourier Transform	0.03 s	No Impact	Low	Small NDZ
	[23]	S-transform	0.03 s	No Impact	Low	Small NDZ
	[24]	Wavelet transform	0.6 s	No Impact	Low	Small NDZ
	[25]	Artificial Neural Network based	0.7 s	No Impact	Low	Small NDZ
	[26]	Support Vector Machine Classifire	-	No Impact	Low	Small NDZ
Remote IDMs	[27]	Power Line Carrier Communication	100 – 300 ms	No impact	None	None
	[28]	Supervisory Control And Data Acquisition	2 s	No impact	None	None

events, dividing further into active and passive methods. Passive methods, though quick and simple, face limitations in detecting events when generation matches load closely, leading to a significant non-detection zone (NDZ) [7]. Active methods introduce perturbations to identify islanding but can impact power quality [7], [8]. Remote IDMs, utilizing communication links for detection, offer enhanced accuracy and minimized NDZ but come with higher costs and complexity, along with vulnerability to communication failures [9].

Remote IDMs such as power line signaling and transfer trip schemes are more effective in detecting islanding events in DC networks than conventional local methods. These communication-based methods use communication links to recognize between islanding and non-islanding conditions. The main advantages of these methods are the secured power quality and zero NDZ. However, communication-based IDMs face several challenges, including the high cost of comprehensive communication infrastructures and complicated implementation. Moreover, due to the risk of communication failure, the effectiveness of these methods cannot be guaranteed [29], [30].

To address the challenge of accurately detection of islanding conditions and ensuring selective protection in DC MGs, there is a growing interest in adopting advanced signal processing methods. These techniques utilize signal processing tools to analyze DC voltage and current, establishing criteria for fault location. Signal processing involves analyzing system output signals to detect faults without requiring a detailed input-output model of the system. Key signal analysis methods include fast Fourier transform (FFT) [31], short-time Fourier transform (STFT) [32], and Hilbert-Huang Transforms (HHT) [33]. The FFT is used to analyze how the frequency content of a non-stationary signal changes over time, offering a more perspective on the data features. STFT, in particular, finds common usage in detecting and categorizing failures in DC MGs due to its ability to overcome Fourier transform limitations related to signal intervals. The S-transform is another signal-processing technique for analyzing non-stationary signals. It can be employed in islanding detection systems to analyze frequency components of signals, aiding in the identification of islanding events [34].

The Wavelet Transform (WT) analysis is a signal-processing technique that has been employed for detecting islanding conditions in power systems [23], [35], [36]. The WT IDM is highly effective at detecting rapid changes in signals because it can accurately identify signals in both frequency and time domains. Reference [34] shows the feasibility of detecting faults by analyzing spectral changes in the frequency components of voltage at the PCC during islanding events. However, WT IDMs used in [34] is an offline method and identify an islanding event only after it has already occurred. This delay in detection might risk disconnecting the main grid from other MGs. Table 1 compares the conventional islanding detection methods (IDMs) in AC/Hybrid Power Systems, and Table 2 provides a summary of the characteristics, advantages, and disadvantages of various IDMs in DC MGs, such as current differential and directional protection, which

TABLE 2. Comparison of common islanding detection methods in DC MGs.

No.	Ref.	IDM	NDZ	DT	EDR[1]	UCL[2]	Cost	Pros.	Cons.
1	[37]	Distance Protection	Large	High	Moderate	Yes	Moderate	Simple	Moderate Accuracy
2	[38]–[40]	Current Differential Protection	Small	High	Moderate	Yes	High	High Selectivity, Robust, Simple	Need synchronized measurements, Communication delays
3	[41]	Over Current Protection	Large	Moderate	High	No	Moderate	Simple	Applicable in low and medium voltages, Moderate accuracy, Low selectivity
4	[42], [43]	Under Voltage Protection	Large	Moderate	High	No	Moderate	Simple	Applicable in low and medium voltages, Low accuracy, Low selectivity
5	[44]	Event-based Protection	Moderate	High	Moderate	No	Low	Less measurement equipment, No need to communication provisions	Low reliability, Not robust against high-impedance faults
6	[45]	Directional Protection	Small	Low	Low	Yes	Moderate	High Sensitivity	Communication delays, Limitations against high resistive faults
7	[46]	dv/dt	Large	Moderate	Moderate	No	Low	High Speed	Not robust against noise, Low accuracy, Limited selectivity by low cable impedance
8	[46]	di/dt	Large	Moderate	Moderate	No	Low	High Speed	Not robust against noise, Low Accuracy, Limited selectivity by low cable impedance
9	[45], [47]	Traveling Waves	Very Small	High	Low	No	Low	High Speed	Low accuracy for long lines
10	[48]	Wavelet Transform	Very Small	Moderate	Low	No	Moderate	Fast Detection	Complex analysis, Not robust against noise
11	[49], [50]	Communication-based	Zero	Moderate	Low	Yes	High	Zero NDZ, No Impact on power quality, Low EDR	Expensive, Complex, Detection might be slower, Interface with other signals
12	[51]	Fourier Transform	Small	High	Moderate	No	Low	Fast Detection	Unstable to resolve transient condition,
13	[31]	S-transform	Small	High	Moderate	No	Low	Fast Detection	It fails under transient disturbances
14	[52]	Artificial Neural Network based	Small	Moderate	Low	No	Low	Hig accuracy, Robust	High computational time for training, The trained network is only accurate for the studied system.

[1]Error Detection Rate, [2]Use of Communication Link.

offer inherent selectivity due to well-defined protection zones.

This paper presents a novel real-time wavelet-based active IDM for fast and reliable identification of islanding events in DC MGs, which considerably reduces the detection time, ensuring fast real-time actions in case of islanding events. The superiority of the proposed method is validated in a DC power system including an infinite DC bus connected to the common DC through the main bidirectional DAB converter. Additionally, three different MGs are connected to the common DC bus employing their respective bidirectional DC-DC converters. In cases where the perturbation signal is detected, the controllers maintain the connection of the main grid to the common DC link, ensuring continuous operation of the system. Conversely, in the absence of the perturbation signal, all bidirectional DC-DC converter controller disconnect their connection to the rest of the system, effectively disconnecting each MG from the common DC bus and the main grid. The discrete nature of the perturbation signal significantly reduces disturbances on the power quality of the system. By combining the advantages of real-time detection, precise and highly reliable detection methods, and low-cost implementation due to the lack of extensive communication infrastructure, this technique offers an enhanced solution for islanding detection in DC MGs. Furthermore, due to the narrow band perturbation signal, this method can distinguish between islanding conditions and any other noise or unwanted signal, proving its robustness. Notably, the method achieves a near-zero NDZ, representing a significant advancement among conventional IDMs.

The subsequent sections of this paper are organized as follows: Section II presents an overview of the studied system. Section III focuses on the model derivation. The methodology employed in the proposed approach is detailed in Section IV. Section V presents simulation parameters. The results and discussion of the proposed IDM are provided in Section VI. The stability analysis of the proposed approach in both island and non-island conditions is presented in Section VII. Finally, Sections VIII and IX belong to the comparison and conclusion, respectively.

II. STUDY SYSTEM

Fig. 1 shows the schematic of a multi-terminal radial DC system that has been used to develop a new islanding detection algorithm in a DC power system. Also, Fig. 2 displays the schematic of the proposed DC power system in "Normal" and "Islanding" operation modes. According to Fig. 2, the proposed system comprises an infinite DC bus that connects to a common DC bus through a DAB converter. Three separate DC MGs are connected to the other side of the common DC bus through their respective bidirectional DC-DC converters. Each MG operates independently with

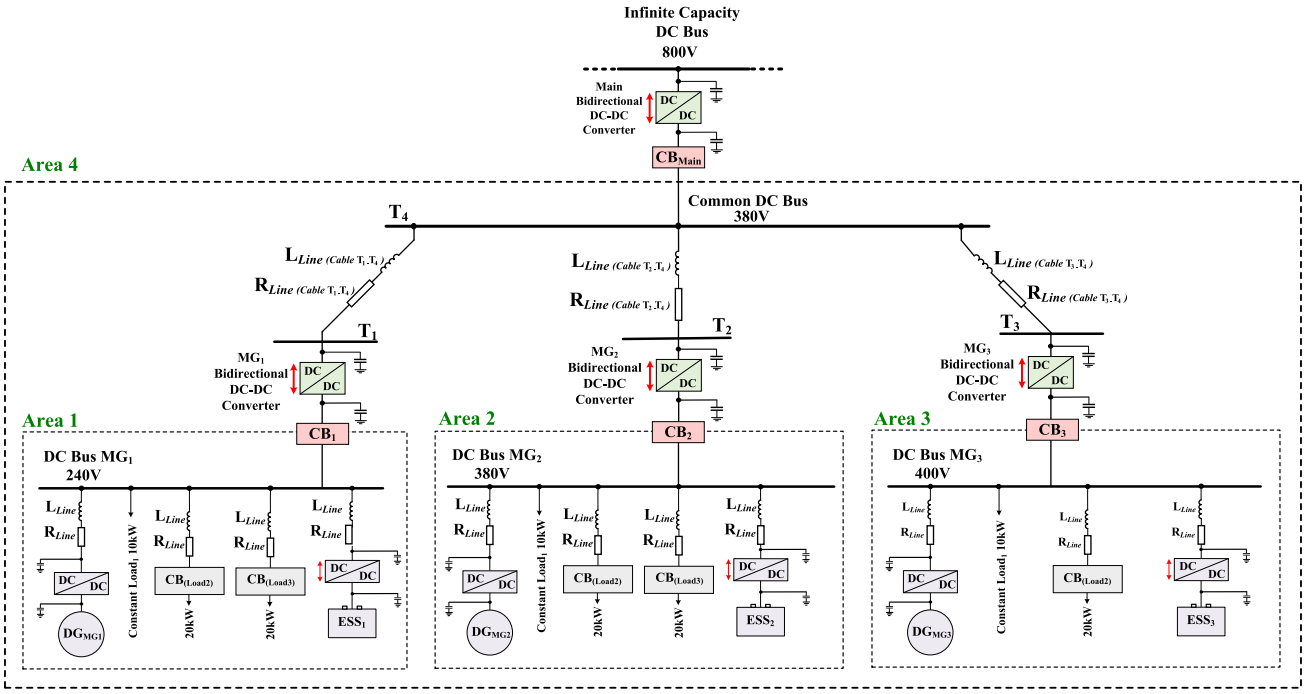

FIGURE 1. The schematic of a four-terminal DC power system.

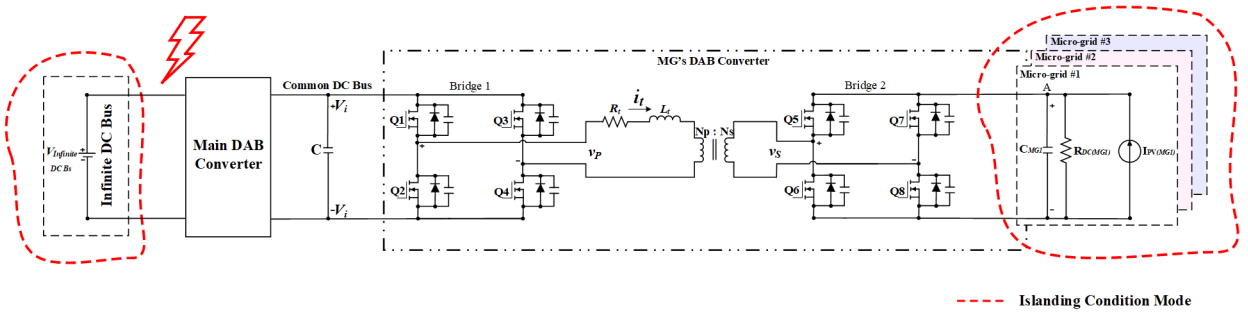

FIGURE 2. Schematic of the proposed DC power system in "Normal" and "Islanding" operation modes.

its power demands and supplies, which may vary over time. Table 3 shows some of the high-level design specifications and modeling parameters used to simulate the MGs and the infinite DC bus. Power lines are modeled using the equivalent series resistance of 0.083 $\Omega.km^{-1}$ and the equivalent inductance of 0.1 $mH.km^{-1}$.

III. MODEL DERIVATION

In this section, the generalized average model is used to model the dynamics of the DAB converter [53], [54], [55], [56]. This technique is based on representing a signal using the Fourier series as follows:

$$x(\tau) = \sum_{-\infty}^{+\infty} \langle x \rangle_k(t) e^{jk\omega_s \tau} \tag{1}$$

where:

$$\begin{aligned} \langle x \rangle_k(t) &= \frac{1}{T} \int_{t-T}^{t} x(\tau) e^{-jk\omega_s \tau} d\tau \\ &= \frac{1}{T} \int_{t-T}^{t} x(\tau) cosk\omega_s \tau d\tau - j \frac{1}{T} \int_{t-T}^{t} x(\tau) sink\omega_s \tau d\tau \end{aligned} \tag{2}$$

Using the dynamical equations of the inductor current and the capacitor voltage, the state equations of the DAB converter presented in Fig.2 can be derived as follows:

$$\begin{aligned} \frac{di_t(\tau)}{dt} &= -\frac{R_t}{L_t} i_t(\tau) + \frac{1}{L_t} S_1(\tau).V_{in}(\tau) \\ &\quad - \frac{N}{L_t} S_2(\tau).V_{DC(MG_1)}(\tau) \\ \frac{dV_{DC(MG1)}}{dt} &= -\frac{1}{R_{DC(MG1)} C_{(MG1)}} V_{DC(MG1)} \end{aligned} \tag{3}$$

TABLE 3. Modeling parameters of the DC power system.

Symbol	Item	Value
$V_{(InfiniteDCBus)}$	Infinite DC Bus Voltage	800 V
$V_{(CommonDCBus)}$	Common DC Bus Voltage	380 V
$V_{(DC-MG1)}$	DC Bus Voltage of Microgrid 1	240 V
$V_{(DC-MG2)}$	DC Bus Voltage of Microgrid 2	380 V
$V_{(DC-MG3)}$	DC Bus Voltage of Microgrid 3	400 V
l_{Line}	Inductance per Kilometer of DC cable	0.10 $mH.km^{-1}$
R_{Line}	Resistance per Kilometer of DC cable	0.083 $\Omega.km^{-1}$
L_{Line} (Cable T1-T4)	Hypothesized Long Distance of DC cable between T1 to T4	10 km
L_{Line} (Cable T2-T4)	Hypothesized Long Distance of DC cable between T2 to T4	15 km
L_{Line} (Cable T3-T4)	Hypothesized Long Distance of DC cable between T3 to T4	50 km
l_{Line} (Cable T1-T4)	Equivalent Inductance of DC cable (T1-T4)	1 mH
l_{Line} (Cable T2-T4)	Equivalent Inductance of DC cable (T2-T4)	1.5 mH
l_{Line} (Cable T3-T4)	Equivalent Inductance of DC cable (T3-T4)	5 mH
R_{Line} (Cable T1-T4)	Equivalent Resistance of DC cable (T1-T4)	0.83 Ω
R_{Line} (Cable T2-T4)	Equivalent Resistance of DC cable (T2-T4)	1.245 Ω
R_{Line} (Cable T3-T4)	Equivalent Resistance of DC cable (T3-T4)	4.15 Ω

$$+\frac{N}{C_{(MG1)}}.i_t(\tau)S_2(\tau)+\frac{1}{C_{(MG1)}}I_{pv(MG1)}(\tau) \tag{4}$$

In a conventional state-space average model, the state variables can be simplified using only the DC terms ($k=0$) of the Fourier series. However, since the transformer current i_t is purely AC, the DC term is zero and there is a large ripple that needs to be modeled. Thus, the average model utilizes more terms in the Fourier series to represent more details in the model. In the case of the DAB converter, it is common to include more terms ($k=0$, $k=+1$, and $k=-1$) in the Fourier series to represent the average values of the state variables. In a continuous-time model, the state-space representation of the systems is given by:

$$\dot{X}(t)=A.X(t)+B.U(t) \tag{5}$$

where matrices X and B are defined as follows and matrix A is presented in (6), shown at the bottom of the next page.

$$X=\begin{bmatrix}\langle V_{DC(MG_1)}\rangle_0\\ \langle i_t\rangle_{1R}\\ \langle i_t\rangle_{1Im}\\ \langle i_t\rangle_0\\ \langle V_{DC(MG_1)}\rangle_{1R}\\ \langle V_{DC(MG_1)}\rangle_{1(Im)}\end{bmatrix}\quad B=\begin{bmatrix}0 & \frac{1}{C_{(MG_1)}}\\ 0 & 0\\ -\frac{2}{\pi.L_t} & 0\\ 0 & 0\\ 0 & 0\\ 0 & 0\end{bmatrix}$$

In the proposed systems at (5), "R" and "Im" represent the real and the imaginary parts of a complex number, respectively. It is assumed that $\langle i_t\rangle_0$ is zero since $\langle i_t\rangle$ has an AC nature and does not have a DC term. Additionally, since the dynamics of $V_{DC(MG1)}$ is much slower than i_t, it can be assumed that the variation of the $V_{DC(MG1)}$ is negligible. Therefore, $\langle V_{DC(MG1)}\rangle_{1R}=\langle V_{DC(MG1)}\rangle_{1Im}=0$. The input capacitance (C_{in}) is relatively large, so the input voltage variation is not significant, and the dynamic of the input capacitor is not considered.

As it can be seen from the equations (5) and (6), the $\langle i_t\rangle_0$, $\langle V_{DC(MG_1)}\rangle_{1R}$, and $\langle V_{DC(MG_1)}\rangle_{1Im}$ are decoupled from the system inputs. Since their initial values are zero, they do not have any variations in time. So, their steady-state values are also zero, and their dynamics are independent of the rest of the system. Accordingly, the dimension of the state-space matrix can be reduced to 3 as represented in (7), shown at the bottom of the next page. The state-space matrix indicates that the system's dynamics can be described using the 0^{th} coefficient of output voltage $V_{DC(MG1)}$, and the 1^{st} coefficients of transformer current as state variables. Including more terms in the Fourier series would increase the model's accuracy, but it would also make the model more complex.

The steady-state equations of the systems can be derived by setting the derivatives of the state variable to zero. By doing that and substituting $i_{t(1R)}$ and $i_{t(1Im)}$ into $V_{DC(MG1)}$, the following equations can be calculated:

$$\begin{aligned}&V_{DC(MG1)}(1+\frac{8N^2R_{DC(MG1)}R_t}{\pi^2(R_t^2+L_t^2\omega_s^2)})\\ &=R_{DC(MG1)}I_{pv1}+\frac{8NR_{DC(MG1)}}{\pi^2}\frac{R_tcos(d\pi)+\omega_sL_tsin(d\pi)}{(R_t^2+L_t^2\omega_s^2)}v_i\end{aligned} \tag{8}$$

As $8R_{DC(MG1)}R_t\le\pi^2(R_t^2+L_t^2\omega_s^2)$, and by assuming $N=1$, equation (8) can be rewritten as equation (9).

$$\begin{aligned}V_{DC(MG1)}&=R_{DC(MG1)}I_{pv1}\\ &+\frac{8N^2R_{DC(MG1)}}{\pi^2}\frac{R_tcos(d\pi)+\omega_sL_tsin(d\pi)}{(R_t^2+L_t^2\omega_s^2)}v_i\end{aligned} \tag{9}$$

Equation (9) is obtained under normal conditions (non-islanding). However, in the event of islanding, the infinite DC bus is disconnected from the rest of the system and this will result in $i_t = 0$. In this scenario, the reflection of i_t on the second side is also zero. Consequently, all parts of I_{pv1} flow into $R_{DC(MG1)}$. The steady-state equation for the islanded DC network is then expressed as follows:

$$V_{DC(MG1)} = R_{DC(MG1)} I_{pv1} \tag{10}$$

Comparison between (9) and (10) shows that during the transition from "normal" to "islanded" mode, the bus voltage $V_{DC(MG1)}$ varies by the term of:

$$\frac{8N.R_{DC(MG1)}}{\pi^2}\left(\frac{R_t cos(d\pi) + \omega_s L_t sin(d\pi)}{(R_t^2 + L_t^2\omega_s^2)}\right)v_i \tag{11}$$

Therefore, the difference between "normal" and "islanded" modes is:

$$\Delta V_{DC(MG1)} = \frac{8N.R_{DC(MG1)}}{\pi^2}\left(\frac{R_t cos(d\pi) + \omega_s L_t sin(d\pi)}{(R_t^2 + L_t^2\omega_s^2)}\right)v_i \tag{12}$$

IV. METHODOLOGY

The system can be operated in two different modes depending on the connectivity of the infinite DC bus to the main DAB converter: normal operation mode and islanding operation mode. Fig. 3(a), and Fig. 3(c) depict the system study in the 'normal operation mode' in the absence and presence of the proposed method, respectively. In the presence of the proposed method, the main DAB converter acts as the primary controller to maintain the voltage of the common DC bus. The controller of the main DAB converter injects a periodic perturbation signal into the system. At each MG terminal (DC link), a local detector measures the voltage and current, transmitting the monitored data through the DC link to the control systems to implement the relevant control algorithm. The presence of the perturbation signal within the DC voltage indicates the normal operation mode.

Fig. 3(b), and Fig. 3(d) illustrate the system study in the "islanding operation mode" without and with the proposed method, respectively. The absence of the proposed perturbation signal indicates that the system is in an islanding condition. After detecting the islanding condition, since power-generating nodes may still be active and contribute to the system during the islanding mode, the main objective is to stop the power-generating nodes as soon as the main grid is absent. Therefore, if the signal is not received, the common DC bus should be de-energized, and each MG should supply its loads.

A. CONTINUOUS WAVELET TRANSFORM (CWT) IMPLEMENTATION

1) USING MORLET WAVELET

In this section, the application of the Morlet wavelet function is discussed. The unique time-frequency localization characteristics of the Morlet wavelet are harnessed to monitor islanding and non-islanding signals effectively. In this method, the input signal is convolved with a well-suited Morlet wavelet. The choice of the Morlet wavelet for this investigation is based on specific reasons [57]:

1) The primary objective of the proposed method is to identify a single-tone frequency signal within the system.

$$A = \begin{bmatrix} -\frac{1}{R_{DC}.C_{(MG1)}} & -\frac{4Nsin(d\pi)}{\pi.C_{(MG1)}} & -\frac{4Ncos(d\pi)}{\pi.C_{(MG1)}} & 0 & 0 & 0 \\ -\frac{2Nsin(d\pi)}{\pi.L_t} & -\frac{R_t}{L_t} & \omega_s & 0 & 0 & 0 \\ -\frac{2Ncos(d\pi)}{\pi.L_t} & -\omega_s & -\frac{R_t}{L_t} & 0 & 0 & 0 \\ 0 & 0 & 0 & -\frac{R_t}{L_t} & \frac{4Nsin(d\pi)\pi.L_t}{} & \frac{4Ncos(d\pi)}{\pi.L_t} \\ 0 & 0 & 0 & -\frac{2Nsin(d\pi)}{\pi.C_{(MG1)}} & -\frac{1}{R_{DC2}.C_{out}} & \omega_s \\ 0 & 0 & 0 & -\frac{2Ncos(d\pi)}{\pi.C_{(MG1)}} & \omega_s & -\frac{1}{R_{DC2}.C_{(MG1)}} \end{bmatrix} \tag{6}$$

$$\frac{d}{dt}\begin{bmatrix} \langle V_{DC(MG_1)}\rangle_0 \\ \langle i_t\rangle_{1R} \\ \langle i_t\rangle_{1Im} \end{bmatrix} = \begin{bmatrix} -\frac{1}{R_{DC}.C_{(MG1)}} & -\frac{4Nsin(d\pi)}{\pi.C_{(MG1)}} & -\frac{4Ncos(d\pi)}{\pi.C_{(MG1)}} \\ -\frac{2Nsin(d\pi)}{\pi.L_t} & -\frac{R_t}{L_t} & \omega_s \\ -\frac{2Ncos(d\pi)}{\pi.L_t} & -\omega_s & -\frac{R_t}{L_t} \end{bmatrix}\begin{bmatrix} \langle V_{DC(MG1)}\rangle_0 \\ \langle i_t\rangle_{1R} \\ \langle i_t\rangle_{1Im} \end{bmatrix} + \begin{bmatrix} 0 & \frac{1}{C_{(MG1)}} \\ 0 & 0 \\ -\frac{2}{\pi.L_t} & 0 \end{bmatrix}\begin{bmatrix} V_{in} \\ I_{pv1} \end{bmatrix} \tag{7}$$

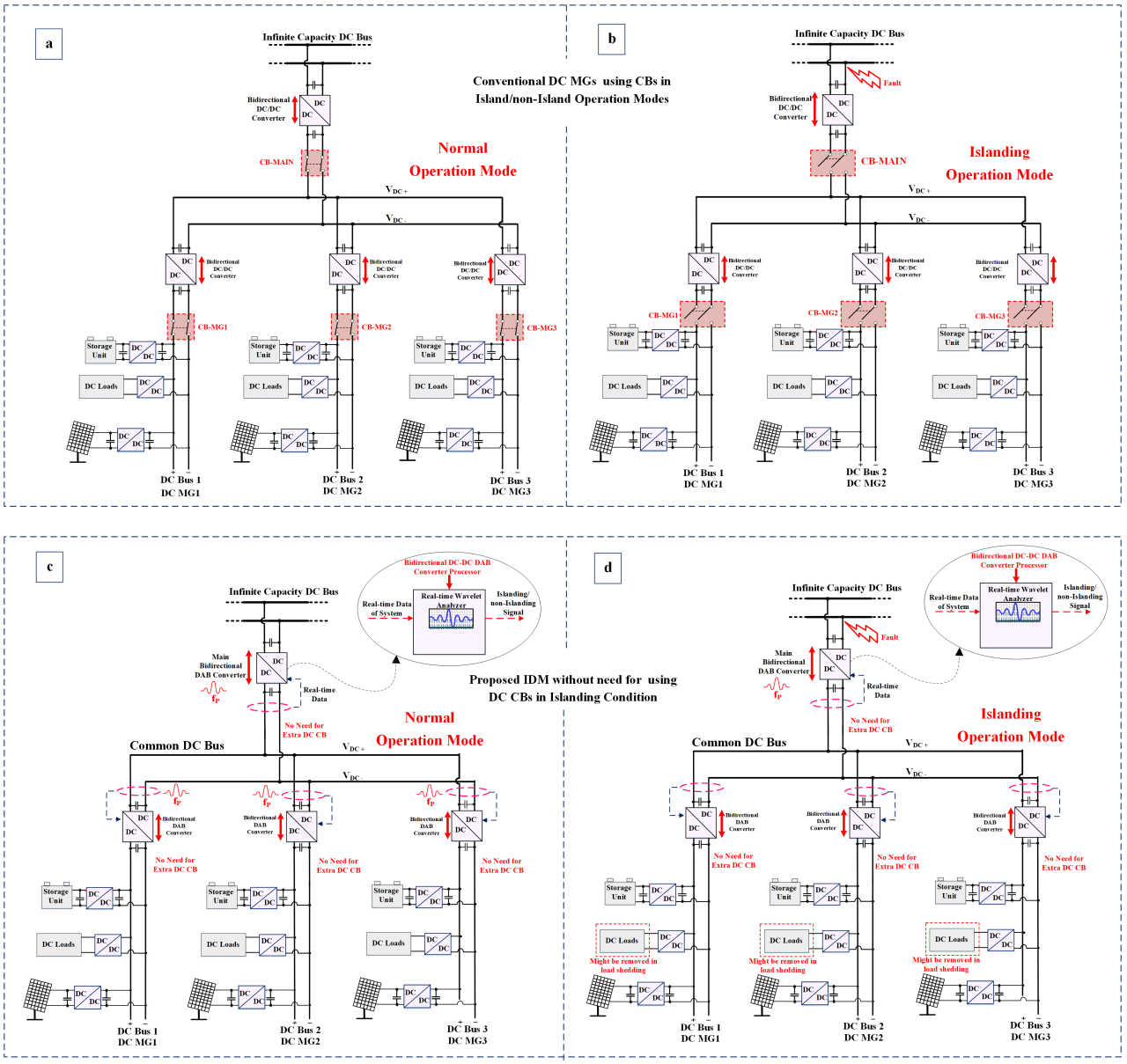

FIGURE 3. Schematic of the radial DC power system using conventional vs. proposed IDM in both normal/islanding operation modes.

2) The Morlet wavelet, functioning as a powerful analytical signal, exhibits a significant correlation with a sine wave.
3) The Gaussian envelope in the time domain enables precise control over the wavelet's time-frequency length.
4) The Morlet wavelet's rapid response characteristic further justifies its selection for this application.

2) MORLET WAVELET TRANSFORM

The wavelet transform which is based on the inner product of the wavelet transform and the signal is defined as (1).

$$\psi_{a,b}(t) = \mid a \mid^{1/2} \psi(\frac{t-b}{a}) \tag{13}$$

where "$\psi(t)$" is the mother wavelet, "a" is the scale factor, and "b" is called the time-location factor. The scale parameter "a" and translation parameter "b" of CWT change continuously. The Morlet wavelet is common for analyzing signals since it is identical to an impulse component. A Morlet wavelet is given by (2).

$$\psi(t) = exp(-\beta^2 t^2/2) cos(\pi t) \tag{14}$$

Considering both dilation factor "a", and translation parameter "b", the Morlet wavelet transform can be defined as:

$$\psi_{a,b}(t) = exp\left[-\frac{\beta^2(t-b)^2}{a^2}\right] cos\left[\frac{\pi(t-b)}{a}\right] \tag{15}$$

As can be seen in (3), three important parameters in a Morlet wavelet are "a", "b", and "β". Different values

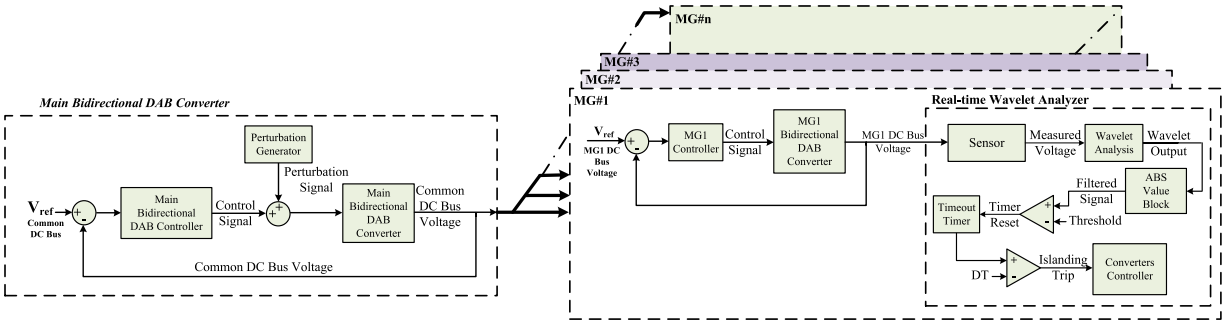

FIGURE 4. Control block diagram of the proposed IDM.

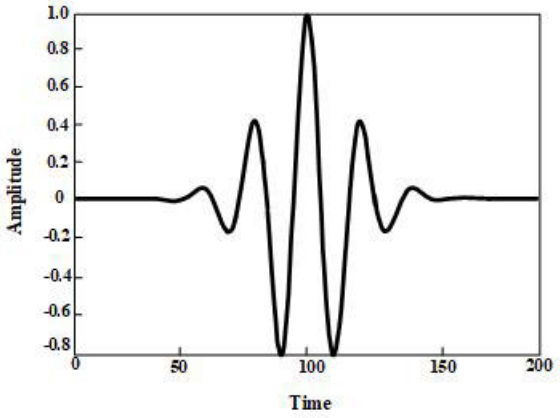

FIGURE 5. Morlet wavelet.

of "a", and "b" result in a shift of the main function in the time domain, and help the proposed signal has a better time resolution. The shape of the Morlet wavelet is also controlled by the parameter "β". The parameter "β" makes a balance between the time and the frequency resolution of the Morlet wavelet. Increasing "β" results in a better resolution in time, and a worse resolution in frequency. When "β" goes toward 0, the Morlet wavelet becomes a cosine function with the best effective frequency resolution. On the contrary, when "β" tends to ∞, the Morlet wavelet has the best time resolution. Accordingly, an optimal "β" provides a proper time-frequency resolution for the proposed signal localized in the time-frequency plane. Fig. 5 illustrates the shape of the Morlet wavelet [58].

Fig. 4 illustrates the control block diagram of the proposed IDM. The main bidirectional DAB converter and its controller are shown on the left. This controller regulates the voltage of the common DC bus by adjusting the converter's control signal. To detect an islanding condition, a high-frequency perturbation signal is injected into this control signal, which is measured at the voltage terminals of each MG. The control signal in the DAB converter is the phase shift (ϕ) between the primary side bridge and the secondary side bridge and it can be defined as $d = \frac{\phi}{\pi}$.

As depicted in Fig. 4, the perturbation signal is added to the desired control variable d. Then, the measured voltage is processed through a wavelet analyzer block. In this block, first, the measured signal is processed in a wavelet analysis block, and then the output of the wavelet analysis passes through the absolute value block to determine whether the perturbation signal is present or not. A compactor determines the existence of the perturbation signal if the output of the absolute value block is above a predetermined threshold. In the existence of the perturbation signal, the timeout timer will be reset before reaching the detection time (DT). In the absence of the perturbation signal, the timeout timer works continually, and it reaches the predefined DT, and the converters' controller will disconnect the common DC bus from all MGs and the main DC bus.

B. PERTURBATION INJECTION

The proposed novel IDM for islanding detection in DC MGs consists of three stages. In the first stage, the main bidirectional DAB converter that connects an infinite DC bus to the common DC bus periodically sends short pulses at a certain frequency on the common DC bus. In the second stage, these pulses are used to send and receive data between nodes. Each MG's DC link is equipped with a detector that measures the DC voltage and it is sensitive to the frequency of this perturbation signal. Finally, in the third stage, when the perturbation signal is present, the MG is connected to the main grid (infinite DC bus), and power can be transferred between the grid and the MGs. The absence of the perturbation signal indicates an islanding condition. After detecting the islanding condition, as power-generating nodes may still be active and contribute to the system during the islanding mode, the main objective is to stop the power-generating nodes as soon as the main grid is absent. Therefore, if the signal is not received, the common DC bus should be de-energized, and each MG should supply its loads. Fig. 6 depicts the flowchart of the proposed method. The injected perturbation signal can be defined as $d = d_0 + A_p sin(\omega_p t)$, where, $\omega = 2\pi f_p, f_p = 1000\ Hz$ and $A_p = 0.03$. By substituting $d = d_0 + A_p sin(\omega_p t)$ into (12), we have:

$$\Delta V_{DC(MG1)}$$

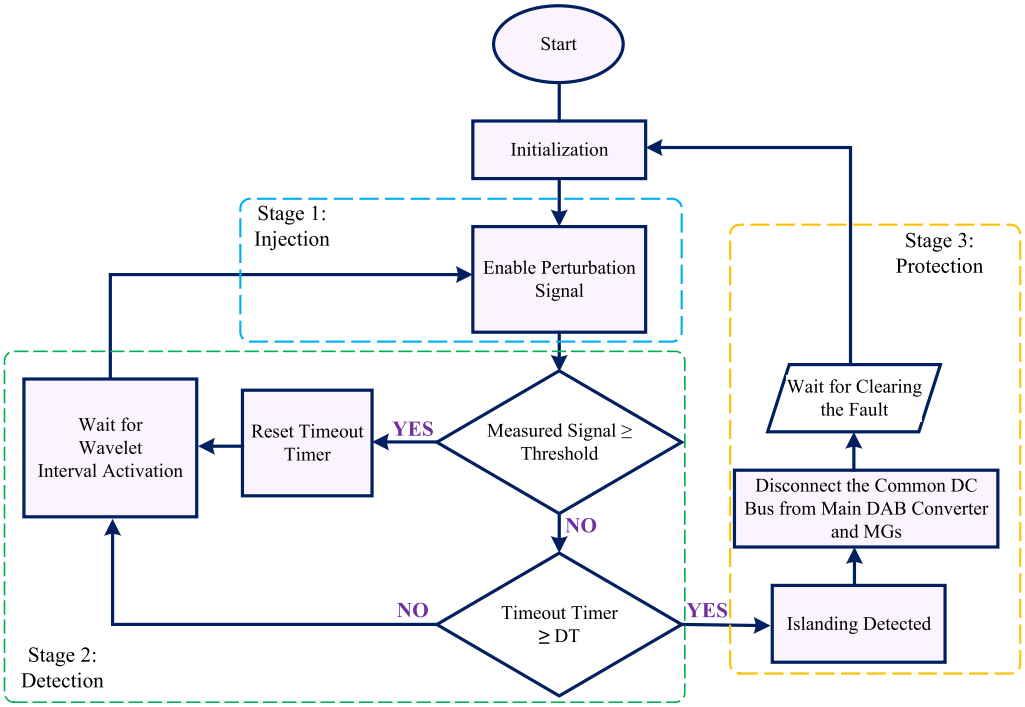

FIGURE 6. Flowchart of the proposed islanding detection algorithm.

$$= \frac{8NR_{DC(MG1)}}{\pi^2} \frac{v_i}{(R_t^2 + L_t^2\omega_s^2)} \times [cos(A_p\pi sin(\omega_p t))(R_t cos(d_0\pi)) + \omega_s L_t sin(d_0\pi)) + sin(A_p\pi sin(\omega_p t))(\omega_s L_t cos(d_0\pi)) - (R_t sin(d_0\pi))] \quad (16)$$

Equation (16) shows that $\Delta V_{DC(MG1)}$ is a function of v_i, f_s, d_0, A_p, f_p, i.e. $\Delta V_{DC(MG1)} = f(v_i, f_s, d_0, A_p, f_p)$. By assuming constant values for v_i, ω_s and d_0 based on the power equation for a fixed design, (16) is only a function of A_p, f_p, so $\Delta V_{DC(MG1)} = f(A_p, f_p)$. Based on the reflection of the frequency and the amplitude of the perturbation signal in the voltage deviations between islanding and non-islanding modes, islanding conditions can be detected in DC MGs.

C. REAL-TIME WAVELET ANALYSIS

To implement the wavelet analysis on the measured signals in the simulation, a C block code is developed. This real-time method utilizes a shifting buffer. Accordingly, new data is added to the first memory cell of the buffer in each sampling sequence, and every other memory cell is shifted, and the last data is discarded. In each sample, the inner product of the wavelet vector and the sampled signal are calculated, and the result is passed through the output of the C block. Based on the presence or absence of the perturbation signal during the DT, it can decide whether to disconnect the MGs from the main grid or not. The proposed real-time wavelet analysis is depicted in Fig. 7.

V. SIMULATION PARAMETER

In this section, the simulation results will be discussed. Table 4 provides the simulation parameters.

A. DETECTION TIME (DT)

The primary challenge facing DC power networks is the absence of comprehensive standard documents. Consequently, in the absence of specific standards for DC power systems, a common practice is to adopt the worst-case scenario of similar AC systems, where the trip time standard is set at 2 cycles (33 ms for 60 Hz) for $137\% \leq V$. As per the guidelines outlined in the IEEE Std. 929-2000, interconnected distributed generation units are mandated to take appropriate action during abnormal conditions. Given the diverse abnormal thresholds, the converter must detect abnormal voltage conditions and respond accordingly. If the perturbation or abnormal condition is not sensed within the specified 33 ms time frame, it indicates that the system is potentially entering an islanding condition. In this scenario, the main grid should disconnect from the common DC bus and any connected MGs promptly. This fast disconnection plays a critical role in maintaining the integrity and stability of the DC power system.

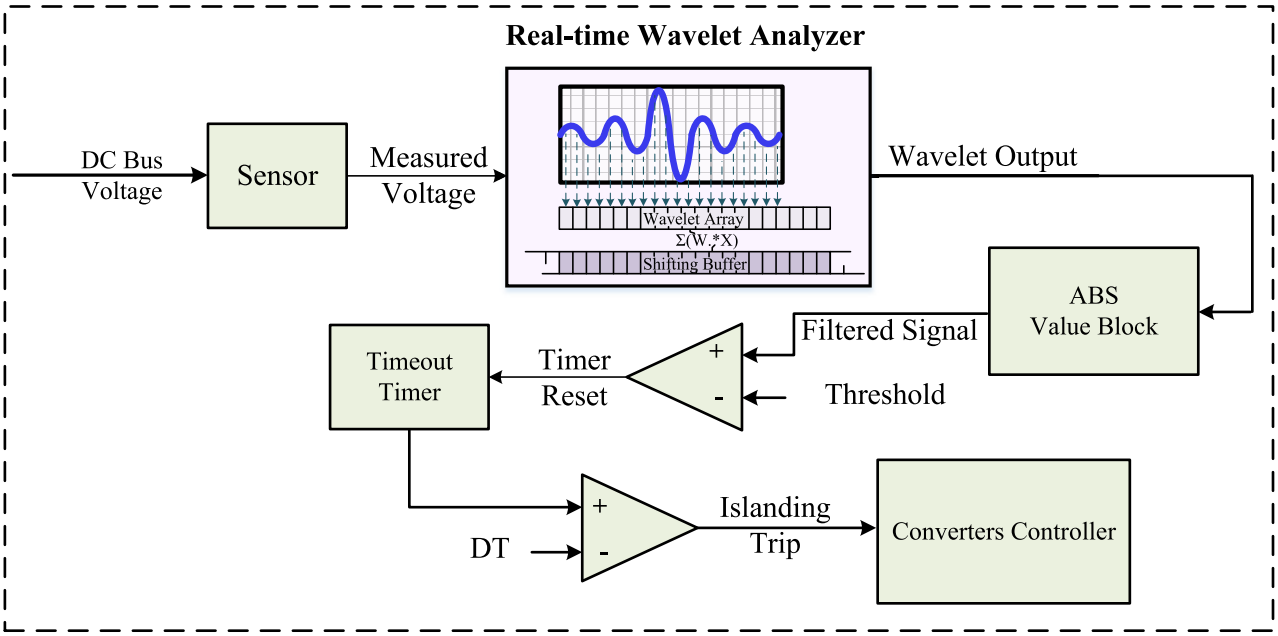

FIGURE 7. Real-time wavelet analysis.

TABLE 4. Simulation parameters.

Symbol	Item	Value	Explanation
f_p	Perturbation Frequency	1000 Hz	Alignment with Signal Characteristics Synchronization with Injection Interval Consistent Signal Pattern Precise Cycle Duration
A_p	Perturbation Amplitude	3%	Voltage Distortion Mitigation Stability Considerations
f_s	Switching Frequency	100 kHz	Converter Specification
T_{Pd}	The perturbation duration	5 ms	Enhanced Noise Differentiation Reduced Risk of Delay Seamless Integration with Wavelet Analysis
$T_{Interval}$	The perturbation Intervals	10 ms	Minimized Disruption Enhanced Reliability
$T_{Islanding}$	Time of Islanding Event	300 ms	Methodology Design

B. PERTURBATION DURATION

Choosing a 5-cycle duration (T_{pd}) for the perturbation signal is crucial to effectively distinguish it from potential noise within the system, whether repetitive or non-repetitive noise occurs at the same frequency as the perturbation signal. In other words, opting for a 5-cycle duration for the perturbation signal is a strategic decision, particularly when compared to shorter durations such as 1 to 4 cycles, which present certain challenges. Within these shorter durations, there is a significant risk that the wavelet might incorrectly interpret noise as the perturbation signal. This issue can lead to delays in detecting critical events like islanding conditions in the system. Conversely, selecting a perturbation signal with a duration of less than 5 cycles introduces the risk of misinterpretation, especially in the presence of non-repetitive noise. In scenarios where the system undergoes islanding, and non-repetitive noise coincides by chance, and considering the absence of a perturbation signal with this non-repetitive noise during islanding, the wavelet may inadvertently delay recognizing the perturbation signal, potentially postponing critical actions by another 33 ms (resulting in a total delay of 66 ms), during which there may be a failure to meet the standard. By specifically opting for a 5-cycle perturbation duration, these risks are mitigated and the wavelet's ability to accurately identify and promptly respond to perturbation signals is enhanced. This approach

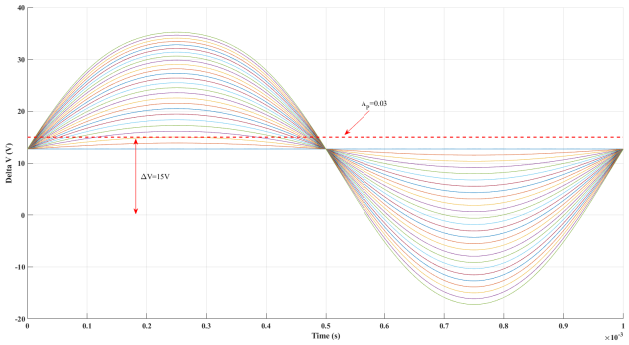

FIGURE 8. Perturbation amplitude.

ensures reliable and timely detection of events, aligning with established standards, and that is precisely the reason for opting for a perturbation signal with more than one cycle repetition.

In addition, the choice of a 5-cycle perturbation signal is rooted in considering the use of a 5-cycle Morlet wavelet as a continuous wavelet transform (CWT). Utilizing a 5-cycle Morlet wavelet complements a 5-cycle perturbation signal seamlessly. The inner product of a 5-cycle perturbation signal with a 5-cycle Morlet wavelet provides comprehensive coverage and yields favorable results. This strategic combination enhances the ability of the proposed method to accurately detect and respond to perturbation signals, aligning to meet established standards.

C. INJECTION INTERVALS

Perturbations are intentionally injected at 10-millisecond intervals ($T_{Interval}$) to maintain balance. Continuous perturbation can disrupt power quality, particularly given the existing noise in the system. Conversely, waiting too long between injections could compromise the method's reliability. In this setup, a perturbation is sent every 10 ms and lasts for 5 ms (or 5 cycles). This means that, in every 10 ms slot, the perturbation signal is active for 5 ms, enters a rest period for the next 5 ms, and then gets ready for the next round. This design carefully maintains power quality standards while effectively managing any unexpected noise in the system. It reduces the impact on power quality and provides sufficient intervals to respond to different types of system noise.

D. PERTURBATION FREQUENCY

The reason behind selecting the perturbation frequency (f_p) is based on the characteristics of a signal with a frequency of 1000 Hz, corresponding to a period of 1 ms. This choice is particularly relevant as perturbations are systematically injected every 10 ms. Within this 10 ms interval, the signal exhibits a pattern of five sine cycles followed by five cycles where it is off. It reveals that the duration of each sine wave within this 10 ms cycle is 1 ms. Therefore, the perturbation frequency is 1000 Hz.

E. PERTURBATION AMPLITUDE

The choice of an amplitude of 0.03 for the perturbation signal is determined by the observed effects of perturbation injection on the common DC bus voltage. Injecting a perturbation into the system leads to distortion in the common DC bus voltage. This understanding informs the decision to select a specific amplitude for the perturbation signal, aimed at achieving the desired level of impact while maintaining system stability. To ensure that the perturbation amplitude (A_p) remains within a reasonable magnitude, careful considerations are made to restrict its range. Through MATLAB simulations, the relationship between A_p and ΔV is examined, as illustrated in Fig. 8. Adhering to standards, a 3.5% tolerance for ΔV is set at 15V. Analysis of the MATLAB graph for a 3.5% ΔV tolerance (15V) reveals that A_p equals 0.035. This careful consideration of A_p ensures that the perturbation-induced distortion in the common DC bus voltage remains within acceptable limits, conforming to industry standards and ensuring the system's stability.

F. THRESHOLD

By adjusting a proper threshold, the system can differentiate the perturbation signal from any other noise and unwanted signals. The reason for setting the threshold at 1.6 is based on a careful consideration of simulation results. The threshold value needs to achieve a fine balance. On one hand, it needs to be high enough to prevent mistakenly identifying small peaks that are due to other noise sources. When the threshold is set too low, there is a risk of misinterpreting these unrelated peaks as injected perturbation signals. This misinterpretation could lead to the inadvertent resetting of the signal when the system enters islanding mode. Conversely, the threshold should not be excessively large to the extent that it overlooks genuine perturbation signals. The design of the threshold has undergone careful consideration through simulations to determine a threshold value that effectively discriminates between the desired perturbation signal and unrelated noise.

VI. RESULTS AND DISCUSSION

To demonstrate the detection of islanded and non-islanded modes using active real-time wavelet analysis, the system being studied was simulated in PSIM. Moreover, to show the 3D scalogram of the wavelet analysis, wavelet calculation was conducted in MATLAB using the DC bus voltage of MG1 as the raw data which should already have the perturbation signal inside it. If the perturbation signal is detected, the system will continue to operate smoothly. If not, the system will enter islanding mode and the converters should disconnect the main DC bus from the common DC bus and MGs. As mentioned earlier, the perturbation signal is a sinusoidal signal with a frequency of 1000 Hz and an amplitude of $A_p = 0.03$. At t =100 ms, this perturbation signal is injected into the controller of the main DAB converter in intervals of 10 ms, as illustrated in Fig. 9(a). As shown in Fig. 9(b), a perturbation enable signal is multiplied by

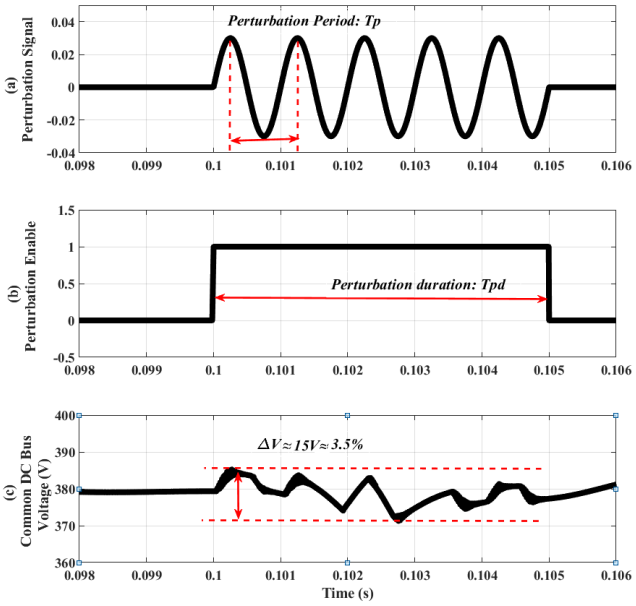

FIGURE 9. (a) Proposed perturbation signal, (b) perturbation enable signal, and (c) common DC bus voltage waveforms.

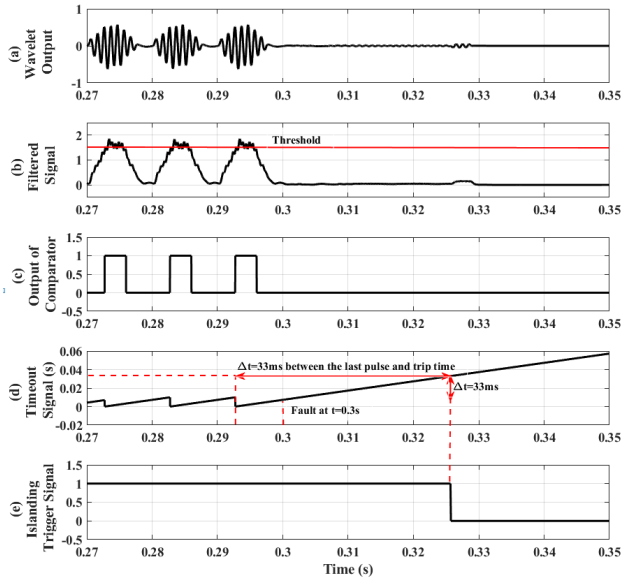

FIGURE 10. (a) Output of C block, (b) Output of amplitude estimator, (c) Output of comparator, (d) Timeout signal, (e) Islanding trigger signal waveforms.

a sinusoidal waveform to control the perturbation signal. Following this, common DC bus voltage is recorded which is shown in Fig. 9(c). The maximum tolerance for voltage in the common DC bus is 0.035, within the standard range.

The wavelet analysis block receives these signals as inputs. Fig. 10(a) shows the output of C block. As Fig. 10(b) depicts, the output is an estimated amplitude signal, which is determined by passing the signal through an absolute value block and a low pass filter. As it can be seen in Fig. 10(b),

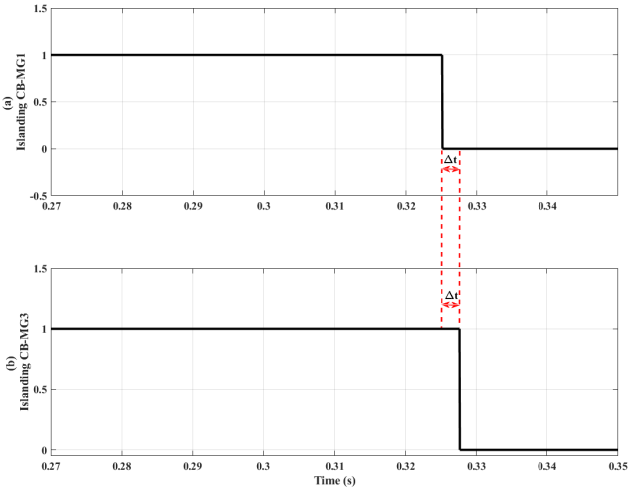

FIGURE 11. Effect of long distance between microgrids and the common DC bus (a) CB-MG1, (b) CB-MG2.

and Fig. 10(c), for further analysis, the output signal is passed through a comparator to compare with a pre-defined threshold. By adapting a proper threshold, the system is able to distinguish between the perturbation signal and any other noise and unwanted signals. Fig. 10(d) shows that the timeout signal is a ramp waveform that is reset every time a perturbation signal is detected. If no signal is received within 33 ms, the timeout signal reaches a timeout threshold and reports an islanding condition. Finally, based on Fig. 10(e), if an islanding condition is detected, the islanding circuit breakers are triggered to stop energizing the common DC bus. The islanding condition occurs at t=300ms after the system start-up. The maximum tolerance for voltage in a common DC bus is 3.5%, which is within the standard range. The output of the comparator, timeout signal, and islanding trigger signal waveforms are shown in Fig. 10.

Fig. 11 shows the effect of long distances on the response time of the CB. This effect comes from the overall line inductance of the interconnections resulting in different delays in the signals. The longer the distance is, the higher the line's inductance; hence, there will be a delay in interconnections and signals. The time difference (Δt) between the two signals illustrated in Fig. 11 depends on the dynamic equations of the transmission line. To calculate that, it is required to solve the proposed dynamic equations in time domains for the mentioned distances in Table 3. To solve these differential equations, the line's equivalent inductance, capacitance, resistance, and transmission line model should be considered. The derived model is also dependent on the type, size, and location of the utilized cables [29], [30].

To conduct wavelet analysis for the 3D Scalogram, the convolution of the Morlet wavelet with the common DC bus voltage at various frequencies and time shifts is essential. As depicted in Fig. 12(a), this approach produces 3D images that depict the frequencies and time intervals of perturbations within this voltage. Notably, at time intervals of 10 ms (e.g.,

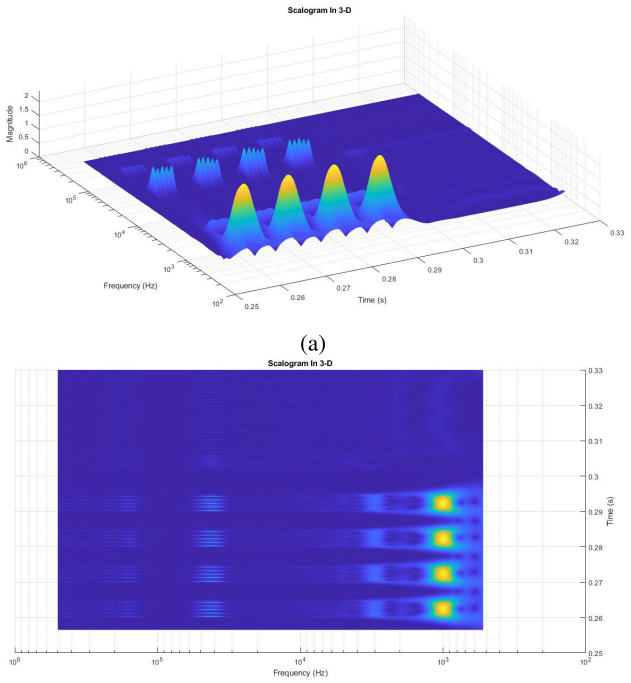

FIGURE 12. Scalogram of the convolution of the Morlet wavelet and the common DC bus voltage, (a) 3D chart, (b) 2D chart.

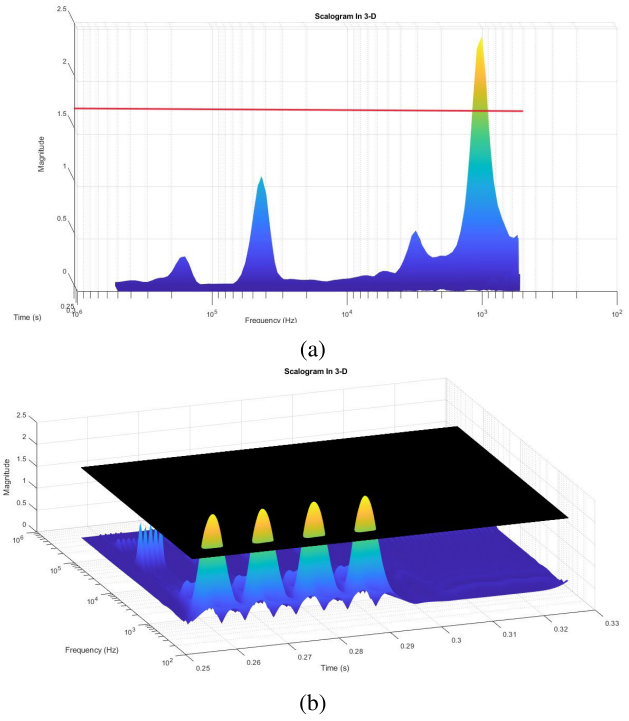

FIGURE 13. A pre-defined threshold in (a) 2D scalogram, (b) 3D scalogram.

t = 0.26s, t = 0.27s, etc.) and around 1000 Hz frequency, the scalogram exhibits peaks higher than 1.6, indicating perturbation signals in these time-frequency intervals. Additionally, Fig. 12(b) presents the 2D Scalogram of the convolution at specific time intervals and frequencies. By establishing a threshold for the convolution value, perturbations in the signal can be identified. This approach is consistent with the PSIM simulation employed in the wavelet analysis block.

Fig. 13(a) and Fig. 13(b) demonstrate that, with an appropriate threshold, the system can differentiate between perturbation signals and other unwanted signals. Finally, as shown in Fig.14, if no signal is received within the specified DT, the timeout signal reaches a timeout threshold and reports an islanding condition.

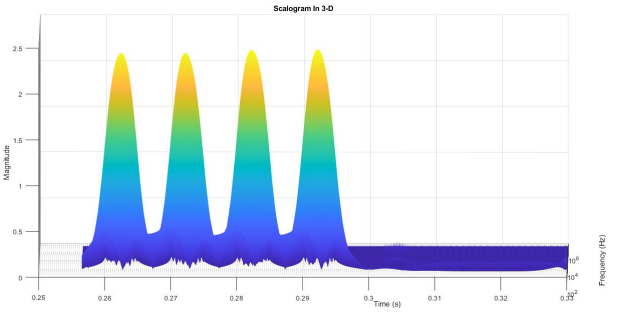

FIGURE 14. Detecting an islanding condition.

VII. SMALL-SIGNAL MODEL

To verify that the proposed method does not compromise the stability of the system, it is essential to employ the small-signal model. This entails deriving the dynamic response of a converter by introducing a small perturbation into the control signal. In (7), when a small perturbation in "d" occurs, the state variables $\langle V_{DC(MG1)}\rangle_0$, $\langle i_t\rangle_{(1R)}$, and $\langle i_t\rangle_{(1Im)}$ deviate from their steady states. The deviations of the state variables from their steady-state value can be expressed as follows:

$$\begin{aligned} \Delta d &= d - D \\ \Delta v_{DC(MG1)_0} &= v_{DC(MG1)_0} - V_{DC(MG1)_0} \\ \Delta i_{t(1R)} &= i_{t(1R)} - I_{t(1R)} \\ \Delta i_{t(1Im)} &= i_{t(1Im)} - I_{t(1Im)} \end{aligned} \tag{17}$$

where the lowercase variables represent large signals, capital letters denote the steady state values, and Δ variables represent small signals.

Equation (7) contains the multiplication of control input and state variables. For a small Δd, the nonlinear term $sin(d\pi).v_{DC(MG1)0}$ can be approximated as follows using (17):

$$\begin{aligned} &sin(d\pi).v_{DC(MG1)0} \\ &= sin(\pi D + \pi\Delta d) \times (V_{DC(MG1)_0} + \Delta v_{DC(MG1)_0}) \end{aligned} \tag{18}$$

Since the multiplication of two Δ variables is very small, we can assume:

$$\begin{aligned} \Delta V_{DC(MG1)_0}\Delta d &\simeq 0 \\ \Delta V_{DC(MG1)_0}(sin(\pi\Delta d)) &\simeq 0 \end{aligned}$$

Similarly, the other nonlinear terms can be calculated using the same approach. Steady-state values of

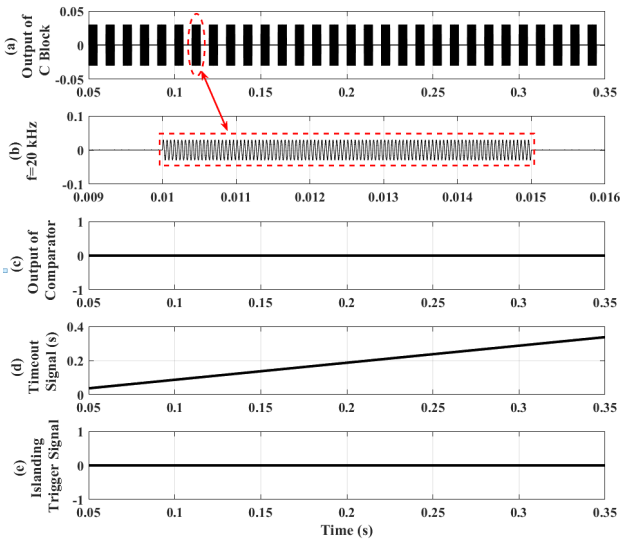

FIGURE 15. Case study 1: f = 20 kHz, amplitude = 3%.

$\langle V_{DC(MG1)}\rangle_0$, $\langle i_t\rangle_{(1R)}$, and $\langle i_t\rangle_{(1Im)}$ can be found from equation (7) by solving:

$$\frac{d}{dt}\begin{bmatrix} V_{DC(MG1)_0} \\ i_{t(1R)} \\ i_{t(1Im)} \end{bmatrix} = 0 \tag{19}$$

Finally, the small signal model is given by (20), shown at the bottom of the next page. The injected perturbation is included in d as $d = d_0 + Asin\omega t$. If there is no perturbation, d is defined as: $d = d_0$.

In the absence of perturbation, the system exhibits a constant matrix A, classifying it as a linear time-invariant (LTI) system.

$$A = \begin{bmatrix} -\dfrac{1}{R_{DC}.C_{(MG1)}} & -\dfrac{4Nsin(d_0\pi)}{\pi.C_{(MG1)}} & -\dfrac{4Ncos(d_0\pi)}{\pi.C_{(MG1)}} \\ \dfrac{2Nsin(d_0\pi)}{\pi.L_t} & -\dfrac{R_t}{L_t} & \omega_s \\ \dfrac{2Ncos(d_0\pi)}{\pi.L_t} & -\omega_s & -\dfrac{R_t}{L_t} \end{bmatrix} \tag{21}$$

The stability analysis for LTI systems is well-established and relatively straightforward. The LTI system is stable if the eigenvalues of matrix A are all negative, i.e. $det(sI - A) = 0 \Rightarrow real(s) < 0$. However, when perturbation is injected, the system becomes a Linear Time-Variant (LTV) system, where the matrix A becomes a function of time. One of the conventional approaches for analyzing stability in Linear Time-Varying (LTV) systems is to define a Lyapunov function from the state variables of the system which is positive definite, and its derivative must be negative definite. This way, it is proven that the overall system is stable. However, defining a Lyapunov function with the aforementioned characteristics is difficult. In the case of an LTV system with periodic features, Floquet theory can also be used as a method to prove the stability of the system by defining a new variable that makes the overall system independent of time (TV), and in that case, the linear systems approaches can be adopted to prove the stability of the system by using the state transition matrix. Again, finding a proper variable to make the system time invariant is a complex task to do.

To address this complexity, an alternative approach is proposed here. Since the time-varying portion of the proposed system in matrix A is a sinusoidal function, it is bounded between -1 and 1, and it cannot have values outside this boundary. Also, another characteristic of a sinusoidal function is that it is uniformly continuous and by analyzing it during one period, we can detect how it behaves over time. Considering all these features, we can divide the sin function over one period to 100 sub-intervals and can assume the system is time-invariant in each sub-interval. Since the system is uniformly continuous and it does not change over time in each sub-interval, the stability of the system can be analyzed using its eigenvalues in each interval, i.e. $det(sI - A') = 0 \Rightarrow real(s) < 0$. We observed that all the eigenvalues are negative for each interval, and we can conclude that the system is stable. Also, the system is uniformly stable and it does not change from one interval to another, so we can conclude that the overall system is stable.

A. COMPARISON OF DIFFERENT WAVELET COEFFICIENTS

Each wavelet transform can be chosen for a particular application based on the signal processing analysis. The Morlet wavelet demonstrates more accurate results than the other continuous wavelet transform because of its Gaussian distribution nature in the frequency domain. As shown in Fig. 9, a perturbation signal is generated at 1 kHz frequency. The amplitude of this perturbation is 3%. Fig. 10 indicates that the perturbation signal detects islanding conditions based on the designed frequency and amplitude. It means that both the designed coefficients and scaled threshold are optimized to detect the islanding condition.

To show that the proposed algorithm is robust to the noise and only works for the designed frequency and amplitude of the perturbation signal, a new simulation has been performed with the perturbation frequency of 20kHz, while the amplitude has remained constant. The result of this condition is illustrated in Fig. 15 When the frequency is higher, the output of the C block cannot detect the perturbation through the common DC bus, so the timeout signal is not reset, and the islanding CB is kept closed. Fig. 16 depicts that a perturbation signal with a frequency of 1 kHz, and an amplitude of 1% is injected into the system. Similar to the previous situation, islanding occurs at t = 300ms after the system start-up. Since the amplitude is lower than the designed value, the islanding signal cannot be detected using the wavelet analysis, and islanding CB is not triggered to disconnect the common DC bus from the rest of the system. This issue may bring hazards to personnel and equipment.

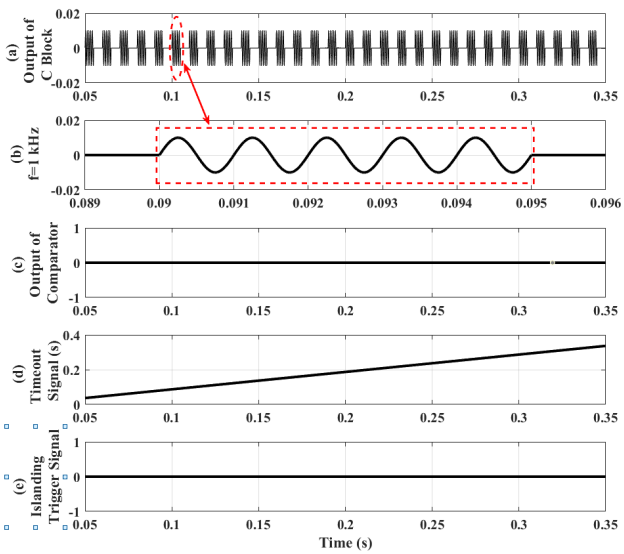

FIGURE 16. Case study 2: f = 1 kHz, amplitude = 1%.

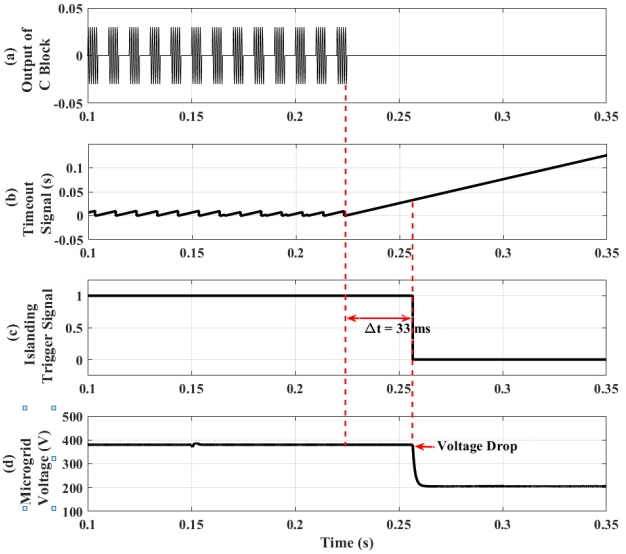

FIGURE 17. Case study 3, f = 1kHz, amplitude = 3%.

So, the importance of designing the optimized coefficients is highlighted in this section.

In the third case as illustrated in Fig. 17, to emphasize the ability of the proposed novel islanding detection method, the islanding event happens at t = 0.23s. In the corresponding MG, the first load is always in the circuit. The second load connects to the circuit at t=0.15s. The total load is now higher than the power capability of MG. Thus, to meet the total load demand, the bidirectional converter should transfer the required power from the common DC bus to the MG. However, the islanding condition happens at 230 ms, and the islanding CB is tripped after 33 ms, causing the MG to be disconnected from the common DC bus, and its voltage is dropped. Table 5 shows the performance of the proposed IDM compared to the other WT-based methods in the literature. As this table presents, the proposed IDM can outperform other methods in different aspects.

VIII. COMPARISON

Table 5 provides a detailed comparison of various IDMs using wavelet-based approaches. The CWT approach offers superior time-frequency localization but comes with a high computational burden. To mitigate this burden in the proposed method, the wavelet function is fixed, and data enters and exits the window in a first-in-first-out (FIFO) manner. This ensures real-time processing without the need to store all the data. The proposed method has a near-zero NDZ, surpassing other methods. Additionally, the detection time is sufficiently low for islanding event detection, meeting the standard for a 33 ms detection time over 2 cycles. An important advantage of this method is that it does not rely on communication links, allowing for local actions to disconnect MGs from the main grid. This independence helps in reducing the overall costs. Another significant advantage is the proposed method's ability to operate even in the power match situation between the main grid and MGs, where no power transfer is necessary. Furthermore, the discrete nature of the perturbation signal considerably reduces its impact on power quality.

IX. CONCLUSION

This paper presents a real-time novel active method designed for fast detection of islanding conditions in DC microgrids

$$\frac{d}{dt}\begin{bmatrix}\Delta v_{DC(MG1)_0}\\ \Delta i_{t_{(1R)}}\\ \Delta i_{t_{(1Im)}}\end{bmatrix} = \begin{bmatrix}-\frac{1}{R_{DC}.C_{(MG1)}} & -\frac{4Nsin(d\pi)}{\pi.C_{(MG1)}} & -\frac{4Ncos(d\pi)}{\pi.C_{(MG1)}}\\ \frac{2Nsin(d\pi)}{\pi.L_t} & -\frac{R_t}{L_t} & \omega_s\\ \frac{2Ncos(d\pi)}{\pi.L_t} & -\omega_s & -\frac{R_t}{L_t}\end{bmatrix}\begin{bmatrix}\Delta v_{DC(MG1)_0}\\ \Delta i_{t_{(1R)}}\\ \Delta i_{t_{(1Im)}}\end{bmatrix} + \begin{bmatrix}-\frac{4Ncos(d\pi)}{\pi.C_{out}}\pi I_{t(1R)} - \frac{4Nsin(d\pi)}{\pi.C_{out}}\pi I_{t(1Im)}\\ \frac{2Ncos(d\pi)}{\pi.L_t}\pi V_{DC(MG1)_0}\\ -\frac{2Nsin(d\pi)}{\pi.L_t}\pi V_{DC(MG1)_0}\end{bmatrix}\Delta d \tag{20}$$

TABLE 5. Citational evaluation of different wavelet-based islanding detection methods.

Ref.	Wavelet Transform	NDZ	DT	Error Detection Rate	Need Communication Link	Cost	Active Passive	Application
[24]	CWT	Large	0.6 s	—	Yes	High	Passive	Grid-tied DG
[59]	DWT	Large	0.05 - 1 s	—	Yes	High	Passive	DG
[60]	DWT	small	27 ms	5% P	Yes	Medium	Active	PV
[61]	DWT	small	1 cycle	50% P	Yes	High	Passive	Wind farm
[62]	PWT	Large	60 ms	—	Yes	High	Passive	Wind Farm
[63]	DWT	small	50 ms	0-20% P	Yes	High	Passive	PV
Prop.	CWT	Near Zero	33 ms	0% P	No	Low	Active	DC MGs

(MGs), eliminating the need for isolators or DC circuit breakers (CBs). Detailed mathematical stability analysis proves that the proposed method ensures system stability, achieving a near-zero non-detection zone (NDZ) and zero false detection. The intentional injection of a narrowband perturbation signal enhances the method's robustness, enabling it to differentiate between islanding events and random fluctuations. Moreover, the method's near-zero NDZ makes it more accurate compared to conventional islanding detection methods. The proposed active strategy, implemented in real-time, minimizes the risk of misidentification under non-islanding conditions while maintaining negligible adverse impacts on power quality. Simulation results validate the performance of the proposed algorithm in detecting the non-islanded/islanded mode of the system, highlighting its potential for seamless integration of DC MGs into modern grids.

REFERENCES

[1] J. Ma, H. Zheng, J. Zhao, X. Chen, J. Zhai, and C. Zhang, "An islanding detection and prevention method based on path query of distribution network topology graph," *IEEE Trans. Sustain. Energy*, vol. 13, no. 1, pp. 81–90, Jan. 2022.

[2] F. S. Al-Ismail, "DC microgrid planning, operation, and control: A comprehensive review," *IEEE Access*, vol. 9, pp. 36154–36172, 2021.

[3] X. Xie, W. Xu, C. Huang, and X. Fan, "New islanding detection method with adaptively threshold for microgrid," *Electr. Power Syst. Res.*, vol. 195, Jun. 2021, Art. no. 107167.

[4] A. Yafaoui, B. Wu, and S. Kouro, "Improved active frequency drift anti-islanding detection method for grid connected photovoltaic systems," *IEEE Trans. Power Electron.*, vol. 27, no. 5, pp. 2367–2375, May 2012.

[5] F. Liu, Y. Zhang, M. Xue, X. Lin, and Y. Kang, "Investigation and evaluation of active frequency drifting methods in multiple grid-connected inverters," *IET Power Electron.*, vol. 5, no. 4, p. 485, 2012.

[6] H. H. Zeineldin and S. Kennedy, "Sandia frequency-shift parameter selection to eliminate nondetection zones," *IEEE Trans. Power Del.*, vol. 24, no. 1, pp. 486–487, Jan. 2009.

[7] Y. Li, P. Zhang, W. Li, J. N. Debs, D. A. Ferrante, D. J. Kane, S. N. Woolard, R. Kalbfleisch, K. B. Bowes, and A. J. Kasznay, "Nondetection zone analytics for unintentional islanding in a distribution grid integrated with distributed energy resources," *IEEE Trans. Sustain. Energy*, vol. 10, no. 1, pp. 214–225, Jan. 2019.

[8] M. Khodaparastan, H. Vahedi, F. Khazaeli, and H. Oraee, "A novel hybrid islanding detection method for inverter-based DGs using SFS and ROCOF," *IEEE Trans. Power Del.*, vol. 32, no. 5, pp. 2162–2170, Oct. 2017.

[9] W. Wang, J. Kliber, G. Zhang, W. Xu, B. Howell, and T. Palladino, "A power line signaling based scheme for anti-islanding protection of distributed generators—Part II: Field test results," *IEEE Trans. Power Del.*, vol. 22, no. 3, pp. 1767–1772, May 2007.

[10] F. Mango, M. Liserre, A. Dell'Aquila, and A. Pigazo, "Overview of anti-islanding algorithms for PV systems. Part I: Passive methods," in *Proc. 12th Int. Power Electron. Motion Control Conf.*, Aug. 2006, pp. 1878–1883.

[11] W. Freitas, W. Xu, C. M. Affonso, and Z. Huang, "Comparative analysis between ROCOF and vector surge relays for distributed generation applications," *IEEE Trans. Power Del.*, vol. 20, no. 2, pp. 1315–1324, Apr. 2005.

[12] F. S. Pai and S. J. Huang, "A detection algorithm for islanding-prevention of dispersed consumer-owned storage and generating units," *IEEE Power Eng. Rev.*, vol. 21, no. 12, p. 67, Dec. 2001.

[13] M. A. Redfern, O. Usta, and G. Fielding, "Protection against loss of utility grid supply for a dispersed storage and generation unit," *IEEE Trans. Power Del.*, vol. 8, no. 3, pp. 948–954, Jul. 1993.

[14] S.-I. Jang and K.-H. Kim, "An islanding detection method for distributed generations using voltage unbalance and total harmonic distortion of current," *IEEE Trans. Power Del.*, vol. 19, no. 2, pp. 745–752, Apr. 2004.

[15] B. Singam and L. Y. Hui, "Assessing SMS and PJD schemes of anti-islanding with varying quality factor," in *Proc. IEEE Int. Power Energy Conf.*, Nov. 2006, pp. 196–201.

[16] M. E. Ropp, M. Begovic, and A. Rohatgi, "Analysis and performance assessment of the active frequency drift method of islanding prevention," *IEEE Trans. Energy Convers.*, vol. 14, no. 3, pp. 810–816, Sep. 1999.

[17] C. Li, C. Cao, Y. Cao, Y. Kuang, L. Zeng, and B. Fang, "A review of islanding detection methods for microgrid," *Renew. Sustain. Energy Rev.*, vol. 35, pp. 211–220, Jul. 2014.

[18] L. A. C. Lopes and H. Sun, "Performance assessment of active frequency drifting islanding detection methods," *IEEE Trans. Energy Convers.*, vol. 21, no. 1, pp. 171–180, Mar. 2006.

[19] C. N. Papadimitriou, V. A. Kleftakis, and N. D. Hatziargyriou, "A novel islanding detection method for microgrids based on variable impedance insertion," *Electr. Power Syst. Res.*, vol. 121, pp. 58–66, Apr. 2015.
[20] V. Menon and M. H. Nehrir, "A hybrid islanding detection technique using voltage unbalance and frequency set point," *IEEE Trans. Power Syst.*, vol. 22, no. 1, pp. 442–448, Feb. 2007.
[21] P. Mahat, Z. Chen, and B. Bak-Jensen, "A hybrid islanding detection technique using average rate of voltage change and real power shift," *IEEE Trans. Power Del.*, vol. 24, no. 2, pp. 764–771, Apr. 2009.
[22] Y. H. Gu and M. H. J. Bollen, "Time-frequency and time-scale domain analysis of voltage disturbances," *IEEE Trans. Power Del.*, vol. 15, no. 4, pp. 1279–1284, Nov. 2000.
[23] P. K. Ray, N. Kishor, and S. R. Mohanty, "Islanding and power quality disturbance detection in grid-connected hybrid power system using wavelet and *S*-transform," *IEEE Trans. Smart Grid*, vol. 3, no. 3, pp. 1082–1094, Sep. 2012.
[24] Y. Zhu, Q. Yang, J. Wu, D. Zheng, and Y. Tian, "A novel islanding detection method of distributed generator based on wavelet transform," in *Proc. Int. Conf. Electr. Mach. Syst.*, May 2008, pp. 2686–2688.
[25] O. N. Faqhruldin, E. F. El-Saadany, and H. H. Zeineldin, "A universal islanding detection technique for distributed generation using pattern recognition," *IEEE Trans. Smart Grid*, vol. 5, no. 4, pp. 1985–1992, Jul. 2014.
[26] M. R. Alam, K. M. Muttaqi, and A. Bouzerdoum, "A multifeature-based approach for islanding detection of DG in the subcritical region of vector surge relays," *IEEE Trans. Power Del.*, vol. 29, no. 5, pp. 2349–2358, Oct. 2014.
[27] W. Xu, G. Zhang, C. Li, W. Wang, G. Wang, and J. Kliber, "A power line signaling based technique for anti-islanding protection of distributed generators—Part I: Scheme and analysis," *IEEE Trans. Power Del.*, vol. 22, no. 3, pp. 1758–1766, Jul. 2007.
[28] I. Pvps, "Evaluation of islanding detection methods for photovoltaic utility-interactive power systems," IEA, Tech. Rep. PVPS T5-09, 2002, vol. 180.
[29] A. Hussain, C.-H. Kim, and A. Mehdi, "A comprehensive review of intelligent islanding schemes and feature selection techniques for distributed generation system," *IEEE Access*, vol. 9, pp. 146603–146624, 2021.
[30] C. N. Papadimitriou, V. A. Kleftakis, and N. D. Hatziargyriou, "A novel method for islanding detection in DC networks," *IEEE Trans. Sustain. Energy*, vol. 8, no. 1, pp. 441–448, Jan. 2017.
[31] D. S. Kumar, D. Srinivasan, and T. Reindl, "A fast and scalable protection scheme for distribution networks with distributed generation," *IEEE Trans. Power Del.*, vol. 31, no. 1, pp. 67–75, Feb. 2016.
[32] T. Tao, "Top right (Fourier transform) top left (Fourier transform)," *Energies*, vol. 30, no. 3, pp. 1–5, 1990.
[33] P. Spanos, "Review of The Hilbert–Huang transform in engineering, edited by Norden E. Huang and Nii O. Attoh-Okine," *J. Waterway, Port, Coastal, Ocean Eng.*, vol. 132, no. 5, pp. 426–427, 2006, doi: 10.1061/(ASCE)0733-950X(2006)132:5(426).
[34] S. R. Samantaray, A. Samui, and B. C. Babu, "S-transform based cumulative sum detector (CUSUM) for islanding detection in distributed generations," in *Proc. Joint Int. Conf. Power Electron., Drives Energy Syst. Power India*, Dec. 2010, pp. 1–6.
[35] M. E. Azzaoui, "An effective islanding detection method with wavelet-based nuisance tripping suppressing," *IEEE Trans. Power Electron.*, vol. 36, no. 12, pp. 13792–13801, Dec. 2021.
[36] E. Kazeminia, S. Eren, and A. Bakhshai, "A novel islanding detection method based on a hybrid algorithm in DC microgrids," in *Proc. IEEE 14th Int. Conf. Power Electron. Drive Syst. (PEDS)*, Aug. 2023, pp. 1–6.
[37] D. Jovcic, D. van Hertem, K. Linden, J.-P. Taisne, and W. Grieshaber, "Feasibility of DC transmission networks," in *Proc. 2nd IEEE PES Int. Conf. Exhib. Innov. Smart Grid Technol.*, Dec. 2011, pp. 1–8.
[38] S. Augustine, J. E. Quiroz, M. J. Reno, and S. Brahma, "DC microgrid protection: Review and challenges," Sandia Nat. Lab.(SNL-NM), Albuquerque, NM, USA, 2018.
[39] G. Liu, F. Xu, Z. Xu, Z. Zhang, and G. Tang, "Assembly HVDC breaker for HVDC grids with modular multilevel converters," *IEEE Trans. Power Electron.*, vol. 32, no. 2, pp. 931–941, Feb. 2017.
[40] E. Christopher, M. Sumner, D. W. P. Thomas, X. Wang, and F. de Wildt, "Fault location in a zonal DC marine power system using active impedance estimation," *IEEE Trans. Ind. Appl.*, vol. 49, no. 2, pp. 860–865, Mar. 2013.
[41] C. Yuan, M. A. Haj-ahmed, and M. S. Illindala, "Protection strategies for medium-voltage direct-current microgrid at a remote area mine site," *IEEE Trans. Ind. Appl.*, vol. 51, no. 4, pp. 2846–2853, Jul. 2015.
[42] S. Beheshtaein, R. M. Cuzner, M. Forouzesh, M. Savaghebi, and J. M. Guerrero, "DC microgrid protection: A comprehensive review," *IEEE J. Emerg. Sel. Topics Power Electron.*, 2019, doi: 10.1109/JESTPE.2019.2904588.
[43] D. Salomonsson, L. Soder, and A. Sannino, "Protection of low-voltage DC microgrids," *IEEE Trans. Power Del.*, vol. 24, no. 3, pp. 1045–1053, Jul. 2009.
[44] F. Yang, N. Xia, and Q.-L. Han, "Event-based networked islanding detection for distributed solar PV generation systems," *IEEE Trans. Ind. Informat.*, vol. 13, no. 1, pp. 322–329, Feb. 2017.
[45] B. Chang, O. Cwikowski, M. Barnes, R. Shuttleworth, A. Beddard, and P. Coventry, "Review of different fault detection methods and their impact on pre-emptive VSC-HVDC DC protection performance," *High Voltage*, vol. 2, no. 4, pp. 211–219, Dec. 2017.
[46] D. Naidoo and N. M. Ijumba, "HVDC line protection for the proposed future HVDC systems," in *Proc. Int. Conf. Power Syst. Technol.*, 2004, pp. 1327–1332.
[47] D. Tzelepis, A. Dysko, G. Fusiek, J. Nelson, P. Niewczas, D. Vozikis, P. Orr, N. Gordon, and C. D. Booth, "Single-ended differential protection in MTDC networks using optical sensors," *IEEE Trans. Power Del.*, vol. 32, no. 3, pp. 1605–1615, Jun. 2017.
[48] N. E. Huang and N. O. Attoh-Okine, *The Hilbert–Huang Transform in Engineering*. Boca Raton, FL, USA: CRC Press, 2005.
[49] X. Liu, A. H. Osman, and O. P. Malik, "Hybrid traveling wave/boundary protection for monopolar HVDC line," *IEEE Trans. Power Del.*, vol. 24, no. 2, pp. 569–578, Apr. 2009.
[50] W. Leterme, J. Beerten, and D. Van Hertem, "Nonunit protection of HVDC grids with inductive DC cable termination," *IEEE Trans. Power Del.*, vol. 31, no. 2, pp. 820–828, Apr. 2016.
[51] Z. Junjie, L. Weixing, and W. Jinyu, "DC fault protection based on change rate of DC voltage in DC grid," *Southern Power Syst. Technol.*, vol. 11, no. 1, pp. 14–22, 2017.
[52] N. B. Hartmann, R. C. dos Santos, A. P. Grilo, and J. C. M. Vieira, "Hardware implementation and real-time evaluation of an ANN-based algorithm for anti-islanding protection of distributed generators," *IEEE Trans. Ind. Electron.*, vol. 65, no. 6, pp. 5051–5059, Jun. 2018.
[53] J. A. Mueller and J. W. Kimball, "An improved generalized average model of DC–DC dual active bridge converters," *IEEE Trans. Power Electron.*, vol. 33, no. 11, pp. 9975–9988, Jul. 2018.
[54] P. F. S. Costa, P. H. B. Löbler, L. Roggia, and L. Schuch, "Modeling and control of DAB converter applied to batteries charging," *IEEE Trans. Energy Convers.*, vol. 37, no. 1, pp. 175–184, Mar. 2022.
[55] S. Goudarzitaemeh and M. Pahlevani, "A bidirectional DC–DC converter with direct power transfer," *IEEE Open J. Power Electron.*, vol. 5, pp. 232–249, 2024.
[56] S. Shao, L. Chen, Z. Shan, F. Gao, H. Chen, D. Sha, and T. Dragičević, "Modeling and advanced control of dual-active-bridge DC–DC converters: A review," *IEEE Trans. Power Electron.*, vol. 37, no. 2, pp. 1524–1547, Oct. 2022.
[57] X. Liu, M. Lewandowski, and N. K. C. Nair, "A Morlet wavelet-based two-point FIR filter method for phasor estimation," *IEEE Trans. Instrum. Meas.*, vol. 70, pp. 1–10, 2021.
[58] Q. Wang, C. Meng, and C. Wang, "Analog continuous-time filter designing for Morlet wavelet transform using constrained L2-norm approximation," *IEEE Access*, vol. 8, pp. 121955–121968, 2020.
[59] C.-T. Hsieh, J.-M. Lin, and S.-J. Huang, "Enhancement of islanding-detection of distributed generation systems via wavelet transform-based approaches," *Int. J. Electr. Power Energy Syst.*, vol. 30, no. 10, pp. 575–580, Dec. 2008.
[60] A. Pigazo, M. Liserre, R. A. Mastromauro, V. M. Moreno, and A. Dell'Aquila, "Wavelet-based islanding detection in grid-connected PV systems," *IEEE Trans. Ind. Electron.*, vol. 56, no. 11, pp. 4445–4455, Nov. 2009.
[61] S. R. Samantaray, T. M. Pujhari, and B. D. Subudhi, "A new approach to islanding detection in distributed generations," in *Proc. Int. Conf. Power Syst.*, Dec. 2009, pp. 1–6.
[62] W. G. Morsi, C. P. Diduch, and L. Chang, "A new islanding detection approach using wavelet packet transform for wind-based distributed generation," in *Proc. 2nd Int. Symp. Power Electron. Distrib. Gener. Syst.*, Jun. 2010, pp. 495–500.
[63] M. Hanif, M. Basu, and K. Gaughan, "Development of EN50438 compliant wavelet-based islanding detection technique for three-phase static distributed generation systems," *IET Renew. Power Gener.*, vol. 6, no. 4, p. 289, 2012.

ELMIRA KAZEMINIA (Student Member, IEEE) received the M.Sc. degree in electrical and computer engineering from Iran University of Science and Technology, Tehran, Iran, with a focus on power system dynamic enhancement by using DPFC. She is currently pursuing the Ph.D. degree in power electronics with Queen's University, Kingston, ON, Canada. Her research is on the subject of islanding detection where she is approaching a new methodology to detect the islanding events in the dc microgrids. Her research interests include dc–dc converters, dc–ac converters, and control and stability of power systems.

SAJJAD GOUDARZITAEMEH (Graduate Student Member, IEEE) received the B.Sc. degree in electrical engineering from the Amirkabir University of Technology (Tehran Polytechnic), Tehran, Iran, in 2014, and the M.Sc. degree in electrical engineering from the University of Tehran, Tehran, in 2017. He is currently pursuing the Ph.D. degree in power electronics with Queen's University, Kingston, ON, Canada. His research interests include unidirectional and bidirectional dc–dc converters, multilevel dc–ac inverters, and advanced control of power converters.

SUZAN EREN (Senior Member, IEEE) received the B.Sc. (Hons.), M.Sc., and Ph.D. degrees in electrical engineering from Queen's University, Kingston, ON, Canada, in 2006, 2008, and 2013, respectively. She is currently an Assistant Professor with the Department of Electrical and Computer Engineering, Queen's University, and a member of ePOWER with the Queen's Centre for Energy and Power Electronics Research Group. Her industrial experience includes collaboration with SPARQ systems in developing their highly efficient solar microinverter. Her research interests include control and signal processing techniques for power converters used in microgrids and renewable energy applications.

ALIREZA BAKHSHAI (Fellow, IEEE) received the B.Sc. and M.Sc. degrees in electrical engineering from Isfahan University of Technology, Isfahan, Iran, in 1984 and 1986, respectively, and the Ph.D. degree in electrical engineering from Concordia University, Montreal, QC, Canada, in 1997. From 1986 to 1993 and from 1998 to 2004, he was a Faculty Member with the Department of Electrical and Computer Engineering, Isfahan University of Technology. He is currently a Faculty Member with the Department of Electrical and Computer Engineering, Queen's University, Kingston, ON, Canada, and a Licensed Professional Engineer in ON. His research interests include high-power electronics, distributed energy generation and conversion, microgrid and smart grid systems, and advanced control theories applied to power electronics converters.